



Published in final edited form as:

Cancer Res. 2022 November 15; 82(22): 4261–4273. doi:10.1158/0008-5472.CAN-21-3214.

Transposon Mutagenesis Reveals RBMS3 Silencing as a Promoter of Malignant Progression of BRAF^{V600E}-Driven Lung Tumorigenesis

Aria Vaishnavi^{1,2,*}, Joseph Juan^{3,4,*}, Maebh Jacob¹, Christopher Stehn¹, Eric E. Gardner⁵, Michael T. Scherzer^{1,6}, Sophia Schuman¹, J. Edward VanVeen^{1,3,7}, Brandon Murphy¹, Christopher S. Hackett³, Adam J. Dupuy⁸, Steven A. Chmura^{3,18}, Louise van der Weyden⁹, Justin Y. Newberg¹⁰, Annie Liu¹, Karen Mann¹⁰, Alistair G. Rust⁹, William A. Weiss^{3,11,12,13}, Conan G. Kinsey^{1,14}, David J. Adams⁹, Allie Grossmann^{1,15}, Michael B. Mann¹⁰, Martin McMahon^{1,3,6,16,17}

¹Huntsman Cancer Institute, University of Utah, Salt Lake City, UT, USA

²Dept. of Cancer Biology, Univ. of Texas, MD Anderson Cancer Center

³Helen Diller Family Comprehensive Cancer Center, University of California, San Francisco, CA, USA.

⁴D2G Oncology, Palo Alto, CA, USA.

⁵Meyer Cancer Center, Weill Cornell Medicine, New York City, NY, USA.

⁶Dept. of Oncological Sciences, University of Utah, Salt Lake City, UT, USA

⁷Dept. of Integrative Biology & Physiology & Jonsson Comprehensive Cancer Institute, University of California, Los Angeles, CA, USA.

⁸Dept. of Anatomy & Cell Biology, University of Iowa, Iowa City, IA, USA.

⁹Experimental Cancer Genetics, Wellcome Trust Sanger Institute, Cambridge, UK

¹⁰Dept. of Molecular Oncology, Moffitt Cancer Center, Tampa, FL, USA.

¹¹Dept. of Neurology, University of California, San Francisco, CA, USA.

¹²Dept. of Pediatrics, University of California, San Francisco, CA, USA.

*Correspondence to: Martin McMahon, Huntsman Cancer Institute, University of Utah, 2000 Circle of Hope Drive, Salt Lake City, Utah 84112, martin.mcmahon@hci.utah.edu.

* Authors contributed equally to this work

AUTHOR CONTRIBUTIONS

This project was initiated at UC San Francisco by J.J. and M.M. in 2011, and was brought to fruition by A.V. and M.M. at Huntsman Cancer Institute, University of Utah. A.V., J.J. and M.M. designed and executed experiments, interpreted data in collaboration with S.C., J.N., A.R., D.A., C.G.K., A.G. AV, JJ and MM co-wrote the manuscript and shepherded it through review. M.J., S.S.S., M.T.S. and J.E.V. assisted with *in vitro* and *in vivo* experiments. E.E.G., C.S.H. and W.A.W. assisted with generation of critical reagents. A.G. assisted with pathological evaluation of tumors. L.v.d.W. performed the linkage-mediated PCR. M.B.M., J.N., A.R., and D.J.A. assisted with sequencing and computational analyses. C.S. helped with data mining of cBioPortal. M.J. and A.L. performed mouse genotyping-related tasks.

Conflicts of interest

Dr. McMahon has served on advisory boards to Genentech Discovery Oncology, Pfizer Oncology, ARO Biotherapeutics, Revolution Medicine.

All additional authors declare no potential conflicts of interest.

13. Dept. of Neurological Surgery, University of California, San Francisco, CA, USA.
14. Dept. of Internal Medicine, University of Utah, Salt Lake City, UT, USA
15. Dept. of Pathology & University of Utah, Salt Lake City, UT, USA
16. Dept. of Dermatology, University of Utah, Salt Lake City, UT, USA
17. Dept. of Cellular & Molecular Pharmacology, University of California, San Francisco, CA, USA.
18. Palo Alto Wellness, Menlo Park, CA, USA

Abstract

Mutationally-activated BRAF is detected in ~7% of human lung adenocarcinomas, with *BRAF^{T1799A}* serving as a predictive biomarker for treatment of patients with FDA-approved inhibitors of BRAF^{V600E} oncoprotein signaling. In genetically engineered mouse (GEM) models, expression of BRAF^{V600E} in the lung epithelium initiates growth of benign lung tumors that, without additional genetic alterations, rarely progress to malignant lung adenocarcinoma. To identify genes that cooperate with BRAF^{V600E} for malignant progression, we employed *Sleeping Beauty*-mediated transposon mutagenesis, which dramatically accelerated the emergence of lethal lung cancers. Amongst the genes identified was *Rbms3*, which encodes an RNA-binding protein previously implicated as a putative tumor suppressor. Silencing of RBMS3 via CRISPR/Cas9 gene editing promoted growth of BRAF^{V600E} lung organoids and promoted development of malignant lung cancers with a distinct micropapillary architecture in BRAF^{V600E} and EGFR^{L858R} GEM models. BRAF^{V600E}/RBMS3^{Null} lung tumors displayed elevated expression *Ctnnb1*, *Ccnd1*, *Axin2*, *Lgr5*, and *c-Myc* mRNAs, suggesting that RBMS3 silencing elevates signaling through the WNT/β-catenin signaling axis. Although RBMS3 silencing rendered BRAF^{V600E}-driven lung tumors resistant to the effects of dabrafenib plus trametinib, the tumors were sensitive to inhibition of Porcupine, an acyltransferase of WNT ligands necessary for their secretion. Analysis of TCGA patient samples revealed that chromosome 3P24, which harbors *RBMS3*, is frequently lost in NSCLC and correlates with poor prognosis. Collectively, these data reveal the role of RBMS3 as a lung cancer suppressor and suggest RBMS3 silencing may contribute to malignant progression.

Keywords

BRAF; lung cancer; transposon; progression

INTRODUCTION

Non-small cell lung cancer (NSCLC) is the leading cause of cancer-related death globally, with adenocarcinoma (LUAD) being the largest sub-type (1). Over the past decade, treatment outcomes have improved for lung cancer patients whose tumors are driven by actionable oncogenic mutations in genes such as Epidermal Growth Factor Receptor (*EGFR*), Anaplastic Lymphoma Kinase (*ALK*), Neurotrophin Tyrosine Kinase Receptor Type 1 (*NTRK1*) or the v-Raf murine sarcoma viral oncogene homolog B (*BRAF*). Indeed, these mutations serve as predictive biomarkers for the use of FDA-approved agents: osimertinib; alectinib, larotrectinib or dabrafenib plus trametinib, respectively (2–4).

However, our understanding of how such oncoproteins promote the initiation, progression and maintenance of lung adenocarcinoma remains incomplete. Moreover, since lung cancers result from the accrual of multiple genetic/epigenetic alterations that cooperate in the conversion of normal lung cells into malignant lung cancer cells, we need a deeper mechanistic understanding of how such cooperation operates at the molecular and cellular levels and how it may influence lung cancer therapeutic strategies.

BRAF^{T1799A} is detected in ~2% of NSCLC patients, translating to ~3,300 patients/year in the US (5,6). As a member of the RAF family of protein kinases, BRAF plays an important role in the activation of the RAS-regulated RAF>MEK>ERK Mitogen Activated Protein Kinase (MAPK) signal transduction pathway. This pathway plays a critical role in normal development and tissue homeostasis, and is frequently dysregulated in human tumorigenesis (7). *BRAF^{T1799A}* encodes BRAF^{V600E}, a constitutively active oncoprotein kinase, mutated in numerous malignancies including melanoma, hairy cell leukemia, colorectal, pancreatic and thyroid cancers (8). The importance of BRAF^{V600E} in cancer maintenance is emphasized through the FDA approval of three pairwise targeted therapeutic combinations that target BRAF^{V600E}>MEK>ERK signaling: 1. Vemurafenib plus cobimetinib; 2. Dabrafenib plus trametinib and; 3. Encorafenib plus binimetinib (9–11). However, although responses to vertical inhibition of BRAF^{V600E} signaling often elicit striking responses, many patients develop lethal drug resistant disease, emphasizing the need for improved therapeutic approaches for these diseases.

We have previously described genetically engineered mice carrying conditional alleles of *Braf* engineered to express normal BRAF prior to CRE-mediated recombination after which BRAF^{V637E} (analogous to human BRAF^{V600E}, nomenclature used hereafter) is expressed at normal physiological, levels in cells in a temporally and spatially restricted manner (12). *Braf^{CAT}* mice were further developed to express both BRAF^{V600E} plus the tdTomato fluorescent reporter from a single bicistronic mRNA upon CRE-mediated recombination (13). Expression of BRAF^{V600E} in alveolar type 2 (AT2) pneumocytes of the mouse lung elicits the development of clonally-derived, benign lung adenomas (12), the malignant progression of which such is constrained by a senescence-like growth arrest triggered by an insufficiency in WNT> β -catenin>c-MYC signaling (14). However, mutationally activated BRAF^{V600E} cooperates with numerous alterations including silencing of TP53 or INK4A-ARF expression, as well as the expression of mutationally-activated PI3-kinase- α (PIK3CA^{H1047R}) or β -catenin (CTNNB1^{ex3}) for malignant lung carcinogenesis (12,15). *Sleeping Beauty*-mediated transposon insertional mutagenesis (*SB-TIM*) has facilitated identification of genes that participate in various aspects of tumorigenesis in GEM models, and was previously used to identify genes that cooperate with BRAF^{V600E} in melanomagenesis (16–19). Here, we employed *SB-TIM* to identify numerous candidate genes that cooperate with BRAF^{V600E} in lung carcinogenesis. Indeed, CRISPR/CAS9 gene editing of one of these genes, *Rbms3*, allowed us to validate it as a novel suppressor of both BRAF^{V600E}- and EGFR^{L858R}- driven lung cancers. Importantly, data from our GEM models are consistent with the observation that loss of some or all of chromosome 3p, where human *RBMS3* is located, is a common event in numerous human lung cancers. These data suggest that *RBMS3* is a previously underappreciated, but frequently silenced lung

cancer suppressor that cooperates with multiple oncogenic events to promote the malignant conversion of normal AT2 cells into lung cancer cells.

MATERIALS AND METHODS

SB tumor sequencing, informatics and statistical analyses

Illumina sequencing—Tumor DNA was extracted from formalin-fixed paraffin-embedded (FFPE) tissues using the Genra PureGene cell kit (Qiagen; 158767) according to the manufacturer's instructions, and barcoded genomic fragments containing transposon-genome junctions sequences were amplified using linker-mediated PCR (LM-PCR) as previously described (20). These products were sequenced on the Illumina 454 platform, from which unique sequencing reads were generated.

Raw processing of sequence data—28 tumors were taken from 10 mice and pair-end sequencing was performed using customized baits and aligned to the mouse genome reference assembly GRcm38 using BWA (version 1.16). The GATK 'indel realigner' was used to realign reads near indels from the Mouse Genome Programme to improve indel/SNP identification. The BAM files were re-sorted to recalibrate quality scores with the GATK 'TableRecalibration' tool. SAMtools 'calmd' was utilized to recalculate the MD/NM tags within the BAM files. Every lane from the same library were merged into a single BAM files using Picard tools (version 1.72) and PCR duplicates were marked using Picard 'MarkDuplicates'.

Merging and Filtering—The BAM files were processed using RetroSeq (version 1.41) to identify pair reads where one read aligned to the reference mouse genome and the other read to the Sleeping Beauty (SB) transposon sequence (Retroseq was operated in "Discovery" mode using the default parameters: Min anchor quality; 20; Min percent identity: 80; Min length for hit: 36). This generated a total of 72,981 individual putative transposon insertion regions (70 across all 28 tumor samples). The sequence and analysis methodologies do not allow the exact SB insertion sites to be identified to the resolution of genomic base pairs hence the location of transposons are referred to as regions as opposed to sites.

Overlapping, individual inverted repeats (IRs) within each sample were merged using bedtools to generate a set of 41,152 IRs. Chromosome four is the donor chromosome for the 6070 transposon line. To reduce the effects of local-hopping that can skew the downstream statistical analysis, all IRs that were located on chromosome four (4,609) were thereby excluded from the analysis. Insertions on the other secondary scaffolds e.x. GL45693, were also excluded. This left a total of 36,510 IRs. Further filtering of the IRs were performed by removing IRs within the regions of two known genes into which the SB concatemer preferentially inserts (on GRcm38:En2; chr5;2816569628173612 and Foxf2; chr13;31625816–31631403.) Nineteen genomic regions reported into which the SB transposon inserts under no selection pressure were also used to exclude IRs that are likely not to be cancer drivers. Following these final filtering step resulted in 36,426 IRs.

DNA sequences corresponding to mouse genomic regions flanking T2/Onc2 insertion sites were mapped using these complimentary standard bioinformatics approaches including the

locus-centric Gaussian kernel convolution, as well as gene-centric common insertion site (gCIS) analysis (16,21). These methods uniformly help identify genomic regions with a higher density of transposon insertions, and strongly suggest these regions contain a potential cancer-relevant gene.

Common insertion sites and trunk driver analysis—Common insertion sites (CIS) were as described previously (22). Briefly, to detect CIS, a GKC method was employed using 15,000, 30,000, 50,000, 75,000, 120,000, and 240,0900 kernel widths. When CISs were detected over several kernel widths, the CISs were merged and the smallest window size is reported. Gene-centric CISs (gCISs) were analyzed as previously described (16). In brief, a gene-centric statistical method was used to identify CIS genes such that genes that had 5 or more read counts, and had insertions in three or more tumors were selected as trunk driver genes. A Bonferroni correction was added to help eliminate false positives, and adjust the p-values (21). This initial list of candidate genes was further analyzed by bioinformatics tools such as Ingenuity Pathway Analysis, as well as STRING and DAVID tools to assess biological relevance, followed by cross-referencing of human tumors analyzed by TCGA.

Vertebrate Animals: Breeding and Experimental Manipulation—All animal care and experimental procedures were approved by Institutional Animal Care and Use Committees (IACUC) at both UCSF and HCI. All mice, whether at UCSF or HCI, were housed in environmentally controlled rooms. *Braf*^{CA} (RRID:IMSR_JAX:017837), *Braf*^{CAT}, *H1^{LSL-CAS9}* (provided by Dr. Monte Winslow, Stanford University; RRID:IMSR_JAX:026816) and *T2/Onc2* (Strain 6070 [B6;C3-TgTn(sb-T2/Onc2)6070Njen] (MGI: 3613048) mice were bred as appropriate and genotyped as previously described (13,23). Mouse health was assessed using the Ullmann-Cullere Body Conditioning Score (BCS) to determine if euthanasia endpoints were met (24), at which point mouse lungs were inflated using either PBS or 10% neutral buffered formalin for perfusion through the larynx, followed by an additional cardiac perfusion of the lung through the right ventricle of the heart until the lungs turned white. Lungs were fixed for 24 hours in formalin prior to transfer to ethanol for paraffin-embedding and the generation of 4µm sections.

Recombinant adeno- or lentiviruses were administered to mice in a BSL2+ room per IACUC protocol and Institutional Biosafety Committee guidelines. Adenoviruses encoding CRE recombinase (Viraquest or the University of Iowa Viral Vector Core) were delivered through intranasal instillation, whereas the lentivirus encoding CRE (described below) was delivered through intratracheal instillation under isoflurane anesthesia (25). Tumor initiation was performed blinded to genotype. All mice were randomized equally among experimental groups based on gender, age, and the correct genotype. All mice used in these experiments had never undergone other experimental procedures. Mice were on a mixed background of C57BL/6, 129, and FVB.

Generation of Rosa-LSL-CAGGS-SB11 mice—The *Rosa26-CAGGS-loxP-STOP-loxP* (64)::*SB* mouse was created by taking a *Rosa26* targeting vector (26,27) and engineered as follows: A construct with an EcoRV restriction site followed by 521bp of homology to the *Rosa26* locus, intron 1 and exon 2 of the mouse Engrailed 2 gene,

the CAGGS promoter, and loxP-flanked EGFP, 2xSV40 polyA sequences, and a bovine Growth Hormone (BGH) polyadenylation sequence was modified by inserting a linker containing NotI, XhoI, and SphI restriction sites into a SalI restriction site downstream of the 3' loxP site. pCMV-SB11 (Addgene plasmid # 26552, Dr. Perry Hackett, University of Minnesota; RRID:SCR_002037) was modified to include a NotI site downstream of the SB11 coding sequence. This vector was digested with EagI and NotI and ligated into the NotI site of the modified *Rosa26* targeting vector. A sequence containing SV40 polyA, a flippase-recognition target (FRT), PGK promoter, neomycin resistance cassette and BGH poly A signal, a second FRT, and 601bp of homology to the *Rosa26* locus was isolated from the initial *Rosa26* targeting vector and ligated into the XhoI site downstream of SB11. This shorter targeting vector was then recombined into a larger *Rosa26* targeting construct containing 3.5kb and 2.9kb of *Rosa26* homology on the 5' and 3' ends respectively. This plasmid was linearized and transfected into E14 mouse embryonic stem (ES) cells. DNA was isolated from selected ES cell clones, digested with ApaI, and screened by Southern blot using a probe (US1) outside of the targeting construct to identify clones with restriction fragment length polymorphisms indicating correct integration of the *CAGGS-LSL-SB11* cassette into the *Rosa26* locus. One clone (A3) was injected into blastocysts to generate 13 chimeric mice. Chimeric males were mated to 129/SvJ females; one chimera was able to propagate the targeted allele through the germline.

Southern blot probe sequence:

US1:

5'ctgggaaggttccttaagaagtattgtctgagaccattctcagtggtcaacaacacttggtcaaaaatttaattctcccctcagag
aatggagtagttactccactttcaagttccttataagcttaccatcaaccttatagctactctagatgtctgaaatttctatcagaaca
aggtagataaaagctggtaggtatacaaacgctagactagttctatccctgacccttaactgctagtatatccgtaggaagttgctta
agtgccactagtagtacc3'

Cell lines, 2D and 3D culture conditions, and imaging—HEK-293T cells (ATCC; CRL-3216) were maintained in DMEM media supplemented with 10%(v/v) fetal bovine serum and 1% penicillin plus streptomycin. All established human cell lines used for these studies have been authenticated by STR profiling and mycoplasma testing is done quarterly using Plasmotest (InvivoGen; rep-pt1).

Organoids were established by dissociating lung tissues minced with a razor and scissors in digestive media comprised of collagenase (400U/ml)(Life Tech #17100–017), dispase (5U/ml)(Corning # 354235), elastase (4U/ml) (Worthington 2279), and DNaseI (0.25mg/ml) (Sigma DN25–100 mg) in advanced DMEM:F12 HAM media in a 37°C shaker for 30 minutes. The resulting single cell suspension was strained using 100, 70 and 40-micron filters. Red blood cell (RBC) lysis was performed at room temperature by incubating each sample with 1x RBC Lysis Buffer (eBioscience; 00–4333-57). Finally, cells were seeded at 50,000 cells/well in matrigel (Corning; #356327 or #354230) in a 24-well plate. Organoids were initially (and experimentally) grown in organoid culture media containing Advanced DMEM/F12 (Gibco), 1x B-27 (Thermofisher; #17504001), N-2 (Thermofisher; #17502001), 1% Penicillin/Streptomycin, 1.25mM N-Acetylcysteine (Sigma-Aldrich; #A0737), 10 nM

Gastrin (Sigma-Aldrich; G9020), 10 μ M Nicotinamide (Sigma-Aldrich; #47865-U), 100 ng/ml EGF (Peprotech; #AF-100-15), 100 ng/ml FGF10 (Peprotech; #100-26), 100ng/mL R-Spondin-1 (Peprotech; #315-32), and 100ng/mL Noggin (Peprotech; #25038) (28,29). To enrich for cells expressing BRAF^{V600E} at organoid initiation, growth factors that activate ERK1/2 signaling (EGF or FGF) were obviated from the organoid media. Following organoid initiation experiments and prior to qRT-PCR, organoids were maintained and expanded in LWRN media (30).

Immunohistochemistry and immunofluorescence of lung sections—

Immunohistochemistry and immunofluorescence was performed as previously described (31), with the following reagents: Xylene (Fisher Scientific; UN1307), Antigen Retrieval: Citrate Buffer pH6 (Sigma-Aldrich; #C9999), Peroxide Block: BLOXALL Blocking Solution (Vector Laboratories; SP-6000-100), Protein Block: Normal Horse Serum Blocking Solution 2.5 (Vector Laboratories; S2012-50); and primary antibodies: c-MYC (Santa Cruz; sc-764; 1:150) (32), pro-SPC (Millipore; AB3786; 1:2000), NKX2.1/TTF-1 (Abcam; 76013-EP1584Y; 1:250; RRID:AB_1310784), EGFR-pY1068 (clone D7A5) XP (CST; 3777; 1:200), pERK T202/Y204 D13.14.4E XP (CST; 4370; 1:600; RRID: AB_10694057), Beta-Catenin D10A8 XP (CST; 8480; 1:50). Secondary antibody: ImmPRESS horse anti-rabbit IgG polymer kit; Peroxidase (Vector Laboratories; MP7401), DAB: ImmPACT DAB Eqv Peroxidase (HRP) Substrate (Vector Laboratories; SK-4103-400), Harris Hematoxylin Solution: (sigma; HHS32), Acid Alcohol (Fisher Scientific; 6769008), Bluing solution: Scott's Tap Water 26070-07 (VWR; 100504-452) and mounted with Permout Mounting Medium (Fisher Scientific; SP15-500). Similarly, immunofluorescence staining of the Sleeping Beauty SB11 transposase was performed by fixing mouse lungs in zinc-buffered formalin, processed and embedded in paraffin, cut into 5-micron sections, and mounted on glass slides. Citrate mediated antigen retrieval was performed, followed by staining with the indicated primary antibody (R&D Systems; #AF2798).

Slide scanning, imaging, and histological analyses and quantification—

Hematoxylin and eosin (H&E) stained slides, and immunofluorescence slides from the SB screen shown in Figure 1 were scanned using an Aperio Scanscope Scanner. Following H&E staining of sectioned lungs from remaining figures, as well as immunohistochemistry, or immunofluorescence analysis, slides of sectioned mouse lungs from each indicated genotype were loaded and scanned automatically using a 3D Histech Panoramic MIDI scanner (ThermoFisher). Slides were imaged and analyzed using CaseViewer Software or the QuantCenter analytical center provided by 3D Histech, and experimental identifiers were blinded for all histological and immunohistochemical analyses. Tumor burden was manually calculated on each lung lobe and total tumor area was compared to total lung area. Tumor diameters were measured using QuantCenter software from 3D Histech. Cellprofiler was used to quantitate median fluorescence intensity with a previously described pipeline following immunofluorescence analysis of mouse tumor bearing lungs (13).

Plasmid cloning, lentivirus production, cell transduction—The CAG-HA-RBMS3-PCDH cDNA expression plasmid was cloned using a cDNA template made from

RNA from the lungs of a wild-type mouse using the Q5 polymerase (NEB) and restriction endonuclease cloning with the following primers: 5': ttttGAATTCCCACCATGTACCCCTATGATGTGCCAGACTACGCCGGCAAACGCCTG GATCAGCCACAA. 3': TtttgccggcgcCTATGGTTTGGACTGTTGGAAGGA. The cDNA was digested with EcoRI and NotI and then inserted into the pCDH mammalian expression vector. Lenti-sgNT/CRE and Lenti-sgLkb1/CRE was a gift from Monte Winslow (Addgene plasmid # 66894 and #66895) (23). Three sgRNAs designed against *Rbms3* were cloned into the pLL3.3 sgRNA-CRE vector by modifying the original sgLkb1 plasmid with the Q5 Site-Directed Mutagenesis kit (NEB; #E0554S). The following sgRNAs against *Rbms3* were used and pooled to make 2 lentiviruses.

Pool 1:

1. GTACACGTACTACTGTCCTC.
2. GAGCACGTCATGGACGCCAC.
3. ATGCAGCCAACTAACATCGT.

Pool 2:

1. ATGCAGCCAACTAACATCGT.
2. TTGGACACGTGATATCCACC.
3. ATCAAGCTATGTCAACCGTA.

Successful clones were verified by Sanger sequencing. Lentiviral supernatants were generated by co-transfection of HEK-293T cells using Transit-X2 (Mirus; #MIR 6004) with a 3-vector lentiviral system: using either the non-targeting sgRNA expression vector or sgRBMS3 sgRNA pool 1 or pool 2 combined with the lentiviral packaging and envelope plasmids pCMV- 8.9 or psPAX2 and pCMV-VSVG. pCMV-VSV-G was from Robert Weinberg (Addgene plasmid # 8454), psPAX2 is from Dider Trono (Addgene plasmid #12260) and pCMV- 8.9 is from PMID: 19561589 (25). Virus was collected 36, 48, 60, and 72 hours-post-transfection, and filtered using a 45-micron filter. Viral supernatants were concentrated by centrifugation at 25,000 rpm for 105 minutes at 4°C. Viral pellets were resuspended in PBS, and stored at -80C. Viral titering was performed using KP1 cells, and flow cytometric analysis of RFP+ cells as previously described (33). $5 \times 10^4 - 1 \times 10^5$ pfu of lentivirus was administered in 75 μ l volume per mouse during intratracheal administration of lentiviruses.

DNA isolation and the Surveyor assay—Lung tumor tissue was micro-dissected and isolated from FFPE tumor blocks and DNA was purified using the QIAamp kit (Qiagen; #56404). Alternatively, DNA was also isolated from cell lines using the DNeasy Blood and Tissue kit (Qiagen; #69504). The Surveyor assay mutation detection kit was used according to the manufacturer's instructions (IDT; # 706025). PCR amplicons of *Rbms3* for the Surveyor assay were generated using the following primers: 5' CTGGATCAGCCACAAATGTACCCCC. 3' TGCTCTGGACCTGGTATGT. The following PCR conditions were utilized with the Q5 polymerase according to the manufacturer's instructions for 25 or 50 μ l reactions (NEB): 98° for 30s, 32 cycles of (98° for 10s, 53°

for 20s, 72° for 40s), 72° for 2 m, and then stored at 4°C for short periods or –20 C for long-term storage.

RNA isolation and qRT-PCR—Lung tumors were isolated by laser-capture microdissection of formalin-fixed paraffin embedded (FFPE) blocks with RNA purified using the RNeasy FFPE Kit (Qiagen; #73504). RNA was purified from cultured organoids following dissociation with TrypLE (ThermoFisher; #12604013), pelleting, and resuspending the organoid cell suspension in Trizol (Invitrogen; #15596026). One-fifth volume of chloroform was added, and the tube was shaken vigorously, followed by centrifugation for 15 minutes at 12,000 x g at 4°C. The aqueous phase was transferred to a new tube, and 10µg of glycogen (ThermoFisher; #R0551) was added. RNA was precipitated with 1/10 volume pH 5.2 3M sodium Acetate (pH 5.2; Thermofisher; catalog #R1181) and 0.5 mL of isopropanol. After mixing the tube was incubated at –80°C for 30 minutes. The mixture was then centrifuged for 10 minutes at 12,000 x g at 4°C, the supernatant removed, and the pellet was washed with 1 mL of cold 75% ethanol. After vortexing, the samples were centrifuged again, before the pellets were air dried, and resuspended in RNase-free water.

cDNA was synthesized using 250ng of template RNA using iSCRIPT reverse transcription supermix (Bio-Rad; # 1708841) according to the manufacturer’s recommended protocol. SSOAdvanced Universal Probes Supermix (Bio-Rad; catalog # 1725280) was used also according to the manufacturer’s protocol. qRT-PCR was performed using Taqman Gene Expression assays (Applied Biosystems; ThermoFisher) and the following 20x probes: *Ppia* (Mm03302254_g1 and Mm02342429_g1) as a housekeeping gene for normalization, *Rbms3* (mm01350499_m1; mm00618362_m1; mm01350496_m1), *Axin2* (Mm00443610_m1), *Lgr5* (Mm00438890_m1), *Ccnd1* (Mm00432359_m1), *C-Myc* (Mm00487804_m1), and *Ctnnb1* (Mm00483029_g1).

cBioPortal analysis of human lung cancer databases—Point mutations were defined as single base-pair alterations and copy number alterations were defined with copy number values less than or equal to –1, consistent with TCGA standards. Search criteria involved listing chromosome arm 3p as a separate field that was queried and automatically aggregated. Individual gene copy number abnormality analysis was conducted through downloading individual patient .cnv files and aggregating manually. Point mutations for individual genes were queried directly within the site interface. Copy number variation (CNV) data were collected via cBioPortal for TCGA-LuSC (n=487) and TCGA-LuAD (n=500) projects from the PanCancer Atlas. From these data, deletions were defined as a copy number equal to –1 and gains defined as copy number equal to 1. Kaplan-Meier curves were generated between cohorts that incurred a deletion of the 3p arm against those that did not incur a deletion.

Data availability

All data and additional resources presented in this manuscript are available upon request to the corresponding author, if access is not already readily available through the indicated, established resources

RESULTS

The *Braf*^{CA}|*SB*|*Lung* (BSL) Insertional Mutagenesis Screen

To conduct the insertional mutagenesis screen, we utilized the following genetic elements: 1. *Braf*^{CA}, a CRE-activated allele of *Braf*(12); 2. *RCL::SB*, *Rosa26-CAGGS-LSL-SB*11, a CRE-activated SB11 transgene in the *Rosa26* locus and; 3. *C4T2/Onc2*, a *T2/Onc2* transposon donor located on chromosome 4. Two cohorts of mice (n=50/cohort) were generated: 1. *Braf*^{CA}; *RCL::SB*; *C4T2/Onc2* (*BRT* mice) and; 2. *Braf*^{CA}; *RCL::SB* (*BR* mice), the latter lacking the *T2/Onc2* transposon. Lung tumorigenesis was initiated by intranasal instillation of 10⁶ pfu of adenovirus encoding CRE recombinase (Ad5.CMV-CRE). In control *BR* mice, the action of CRE recombinase delivered to the lung results in co-expression of BRAF^{V600E} plus SB11 without the *T2/Onc2* transposon, which is only present in the *BRT* mice. Initiated mice were monitored for signs of lethal lung tumorigenesis for 250 days (Fig. 1A). As anticipated, control *BR* mice did not develop disease over the monitoring period, whereas ~70% of *BRT* mice developed end-stage pulmonary disease as evidenced by labored breathing and/or loss of body weight requiring euthanasia. Median survival of initiated *BRT* mice was 205 days compared to 338 days for the *BR* mice (Fig. 1A, p=0.00000383). These data suggested that SB-mediated mobilization of the *T2/Onc2* transposon dramatically accelerated malignant progression of BRAF^{V600E}-driven lung tumorigenesis in *BRT* mice.

At euthanasia, mice were subjected to necropsy revealing that the lungs of *BRT* mice displayed histological evidence of malignant lung cancer *in situ* whereas the lungs of *BR* mice exclusively contained benign adenomas (Fig. 1B). *BRT* mice developed a wide range of tumor grades from benign adenomas to adenocarcinomas (Figs. 1B–D). To identify sites of *T2/Onc2* insertion in the mouse genome, formalin-fixed, paraffin-embedded (FFPE) tissue from 28 individual lung cancers (from 10 mice) were micro-dissected from H&E-stained sections. Tumors from within the same mouse were selected for microdissection based on higher tumor grade (adenocarcinoma), larger tumor size, and detection of the SB transposase (by immunofluorescence; Fig. 1E). *T2/Onc2* chromosomal insertion sites in genomic DNA of these tumors were identified by splinkerette PCR as described previously (34).

Collectively, a pool of bioinformatics analyses, tailored strategically towards SB mutagenesis screens, identified a stratified list of genes that cooperated with BRAF^{V600E} to promote lung tumor progression in a statistically robust manner (Fig. 2 and Table 1). Bioinformatic analysis of the insertion sites suggested that most of the identified genes were likely inactivated by the *T2/Onc2* transposon insertions consistent with our previous SB|*Braf* screen in melanoma (p < 0.005 ; Table 1) (16). Ultimately, this *SB*-TIM screen identified numerous candidates that might cooperate with BRAF^{V600E} in driving malignant lung carcinogenesis.

Rbms3 is a tumor suppressor that cooperates with BRAF^{V600E} in lung carcinogenesis—The two most significantly enriched common insertion sites (CIS) identified in this screen were *Foxp1* and *Rbms3*, which carried 17 and 16 SB insertions respectively (Figs. 2A–C). RBMS3 is a single-stranded RNA binding protein that has been implicated as a potential tumor suppressor in a number of malignancies, including

squamous cell lung cancer (35–42). Furthermore, RBMS3 is implicated as a regulator of WNT signaling, a pathway shown to play critical roles in normal lung development and homeostasis, as well as progression of KRAS^{G12D}- or BRAF^{V600E}-driven lung cancer (14,43–46).

To assess the potential tumor suppressor activity of RBMS3 in BRAF^{V600E}-driven lung carcinogenesis, lentiviral vectors expressing CRE recombinase and either a non-targeting control sgRNA (sgNT) or sgRNAs targeting *Rbms3* were generated (23). Lentiviral supernatants were introduced by intratracheal intubation into the lungs of mice that carried the *Braf^{CAT}* allele, or an *H1^{LSL-CAS9}* allele that allows for CRE-mediated CAS9 expression from the *Hipp11 (H11)* “safe-harbor” locus, either alone or in combination (23). These mice were euthanized at 11 weeks post-initiation for assessment of lung tumorigenesis and evaluated for differences. Infection of *Braf^{CAT}* (B) mice with sgRbms3-CRE virus or of *Braf^{CAT}; H1^{LSL-CAS9}* (BC) mice with sgNT-CRE virus led to the development of benign BRAF^{V600E}-driven lung tumors, as expected (Figs. 3A & B). Strikingly, infection of BC mice with sgRbms3-CRE virus resulted in a significant increase in overall lung tumor burden as well as a significant increase in tumor diameter compared to relevant controls ($p < 0.0001$; T-Test) (Figs. 3C–F). Importantly, no lung tumorigenesis was observed in the *H1^{LSL-CAS9}* (C) mice infected with sgRbms3-CRE virus control group (Fig. 3D). These data suggest that RBMS3 silencing was sufficient to bypass the senescence-like growth arrest observed in benign BRAF^{V600E}-induced lung tumors (12,14). Analysis of genomic DNA isolated from large tumors confirmed CAS9-mediated editing of the *Rbms3* gene (Supp. Fig. 1A). Moreover, unique, micro-dissected tumors also displayed a significant decrease of *Rbms3* mRNA expression compared to controls (Supp. Fig. 1B). Collectively, these data suggest that: 1. *Rbms3* was appropriately edited *in vivo* models using CRISPR/CAS9 editing technology; 2. CRISPR/CAS9-mediated *Rbms3* gene editing resulted in substantially reduced *Rbms3* mRNA expression and; 3. RBMS3 silencing promoted the progression of BRAF^{V600E}-driven lung tumors.

Histological examination of BRAF^{V600E}-driven lung tumors in this study was consistent with previous observations that such tumors are benign adenomas displaying characteristic cytomorphological features with a discreet papillary structure, a central fibrovascular core and with well-circumscribed borders (Supp. Figs. 2A–B) (12,14). Interestingly, the larger BRAF^{V600E}-driven lung tumors (>1mm) that emerged in the context of reduced *Rbms3* expression displayed clear evidence of cancer progression including poorly circumscribed borders, increased nuclear:cytoplasmic ratio, and avascular neoplastic nests free floating in air spaces (Supp. Figs. 2C–F). Importantly, we observed a distinct micropapillary architecture previously shown to be indicative of malignant adenocarcinoma of the lung in patients whose cancers are driven by EGFR, KRAS or BRAF oncoproteins (Supp. Figs. 2E–F) (47). This distinctive phenotype suggests that expression of BRAF^{V600E} in combination with RBMS3 silencing in the mouse lungs mimics key features of human BRAF^{V600E}-driven lung adenocarcinomas. These data are consistent with the hypothesis that RBMS3 is a tumor suppressor, such that its reduced/silenced expression promotes lung cancer progression.

As an additional approach to test oncogenic cooperation between BRAF^{V600E} expression and RBMS3 silencing we developed a mouse lung organotypic model system as a useful and relevant complement to our *in vivo* studies (28,48,49). When single cell suspensions of normal mouse lung are seeded in matrigel in the presence of: R-Spondin-1; Noggin; EGF and FGF10, organoids will develop over the course of approximately 7 days. Consequently, we generated single-cell suspensions from lungs of *BC* mice infected with either sgNT-CRE or sgRbms3-CRE viruses. After one week of culture, organoids established from *BC* mouse lungs in which BRAF^{V600E} expression is combined with RBMS3 silencing were significantly larger than those observed with BRAF^{V600E} expression alone (p<0.0001; T test) (Figs. 4A & 4B). Furthermore, as anticipated, organoids derived from *BC* mice infected with sgRbms3-CRE demonstrated lower *Rbms3* mRNA expression compared to either control or to cells with ectopic expression of *Rbms3* (Fig. 4C). These data provide additional evidence that RBMS3 silencing cooperates with BRAF^{V600E} to promote lung organoid growth *in vitro* consistent with the *in vivo* experiments described above.

Rbms3 cooperates with EGFR^{L858R} in lung carcinogenesis—To determine if the cooperation observed between BRAF^{V600E} and RBMS3 silencing was specific to BRAF^{V600E}, we employed a GEM model of EGFR^{L858R}-driven lung tumorigenesis (50). To that end we used mice carrying *SPC::CRE-ER^{T2}+*, *Rosa26^{CAGs-LSL-rtTa3}*, *TetO::EGFR^{L858R}* that either did (*SREC*) or did not (*SRE*) carry the *H1^{LSL-CAS9}/+* allele. In this model, EGFR^{L858R}-driven lung tumorigenesis can be initiated by the activation of CRE-ER^{T2} in AT2 cells leading to induced expression of the reverse tetracycline transactivator (rtTa3) from the *Rosa26* locus, or Cre. As previously described, subsequent addition of doxycycline to initiated mice leads to induced expression of EGFR^{L858R} in AT2 cells and lung tumorigenesis (50). The lung epithelium of initiated *SRE* or *SREC* mice was infected with lentiviruses expressing either a control sgRNA (sgNT) or one targeted against *Rbms3* as described above (Fig. 3). Here, tamoxifen was not administered to induce SPC specific delivery of CRE Recombinase, but minor leakiness may have occurred. Indeed, RBMS3 silencing cooperated significantly to accelerate EGFR^{L858R}-driven tumorigenesis, compared to relevant controls where *Rbms3* was not altered (Figs. 5A–D) (T-test; p < 0.0001). Combined expression of EGFR^{L858R} with RBMS3 silencing led to diffuse replacement of the lung parenchyma with adenocarcinoma, and neoplastic cells arranged in disorganized clusters that replaced alveolar air spaces that displayed evidence of incited microhemorrhages (Supp. Figs. 3A–F). Cells in these tumors displayed expression of NKX2.1 and pro-Surfactant Protein C, markers of AT2 cell identity and well-differentiated lung adenocarcinoma (Supp. Figs. 3G–J). Interestingly, lung tumors with combined EGFR^{L858R} expression and RBMS3 silencing displayed higher levels of phosphorylated EGFR and phosphorylated ERK1/2 compared to the relevant sgNT controls (Fig. 5E–H). We also observed that *SREC* mice initiated with sgRbms3 compared to sgNT controls (Supplementary Fig. 3K&L) harbored higher expression levels of β-Catenin protein by immunohistochemistry. Taken together, these data indicate that RBMS3 silencing cooperates with multiple drivers of lung tumorigenesis, expanding its relevance from just BRAF^{V600E} to EGFR^{L858R}.

To elucidate the mechanism(s) by which RBMS3 silencing promotes the progression of BRAF^{V600E}-driven lung tumors, we considered previously reported mechanisms of RBMS3 action. It has been reported that RBMS3 binds to the 3' UTR of *c-MYC* mRNA such that RBMS3 silencing might lead to elevated expression of *c-MYC*, or β -Catenin, a key effector of the WNT signaling pathway (14,35,37–40,42–46). When tissue sections were analyzed by immunofluorescence we observed a robust increase in β -Catenin (CTNNB1) expression in BRAF^{V600E}-driven lung tumors without RBMS3 (Figs. 6A–C). To expand on this, we evaluated organoids from *BC* mouse lungs carrying either sgNT or sgRbms3 for differences in mRNA expression of components and transcriptional targets of the WNT signaling pathway, or specifically β -Catenin/TCF/LEF. Here, we identified a significant increase in relative gene expression of *Ctnnb1*, as well as known target genes: *Ccnd1*, *Axin2*, *c-Myc*, and *Lgr5* (Fig. 6D) in sgRbms3 *BC* organoids, suggesting that RBMS3 silencing promotes WNT pathway signaling, a pathway known to be rate-limiting for progression of BRAF^{V600E}-driven lung tumors (14).

Vertical inhibition of BRAF^{V600E} signaling with dabrafenib + trametinib (D+T) is the standard of care for this molecularly defined subset of lung cancer patients, so we sought to explore the consequences of RBMS3 silencing on pathway targeted therapies against BRAF^{V600E} (D+T), or with LGK974 (a Porcupine/WNT pathway inhibitor). To that end, *BC* mice were initiated with lenti-CRE vectors that carried either sgNT or sgRbms3 and, six weeks post-initiation, such mice were randomized for treatment with: 1. Vehicle control; 2. D+T or; 3. LGK974 for a fixed period of 5 weeks at which time mice were euthanized and lung tumor burden was quantified. This revealed that while sgNT *BC* tumor-bearing mice were sensitive to D+T as expected, whereas LGK974 had only a modest effect on tumor burden, but importantly, lung tumors initiated in *BC* mice with sgRbms3-CRE demonstrated resistance to the anti-tumor effects of D+T, but displayed striking sensitivity to the anti-tumor effects of LGK974 (Figs. 7A–H). Immunohistochemical analysis of pERK1/2 in tumors of drug treated mice revealed potent MAPK pathway suppression with D+T compared to vehicle controls, but maintained positive pERK staining when treated with LGK974 (Fig. 7I–N). Moreover, immunohistochemistry revealed that *BC* lung tumors initiated with Rbms3-CRE displayed readily detectable expression of SPC and NKX2.1, suggesting that they maintained a well-differentiated state (Supp. Figs. 4A–L). Importantly, SREC mice that are RBMS3^{Null} compared to NT controls (Supplementary Fig. 3K&L) revealed higher levels of β -Catenin protein by immunohistochemistry. Similarly, *BC* mice treated with vehicle also revealed higher β -Catenin protein expression, further supporting upregulated expression of β -Catenin where RBMS3 expression is silenced (Supp. Fig. 4M–R; compare panels N to M, P to O, and R to Q). Collectively, this data reveals that RBMS3 silencing was sufficient to promote resistance to D+T, and it appeared to enhance the sensitivity of BRAF^{V600E}-driven lung tumors to Porcupine inhibition with LGK974.

Finally, to assess the possible prevalence of alterations in *RBMS3* in human lung cancer, we evaluated existing patient data from The Cancer Genome Atlas (TCGA) available through the cBio portal for cancer genomics (51,52). Initial analysis indicated that point mutations in the *RBMS3* gene are rare in this collection of human lung tumors. Analysis of changes in the region of chromosome 3p24 where *RBMS3* is located in lung cancer patients gave a striking pattern of changes (Supp. Fig 5A). We documented that >45%

of lung adenocarcinomas and >89% of lung squamous carcinomas displayed loss of copy number of *RBMS3* on chromosome 3p24 (Supp. Figs. 5B–D). However, it must be noted that the majority of these cases showed loss of the entire 3p arm of chromosome 3, not focal deletions of *RBMS3*. Specifically, 77.8% of squamous cell carcinoma patients (87% of the patients who lost *RBMS3*) and 38.7% of adenocarcinoma patients (86% of patients who lost *RBMS3*), showed loss of the entire 3p arm (Supp Fig. 5). Interestingly, these copy number alterations in *RBMS3* frequently co-occurred with both *EGFR* or *BRAF* oncogenic mutations in these patients (Supp. Fig. 5F). Furthermore, there was a correlation between loss of chromosome 3p in patients and poorer prognosis for such lung cancer patients compared to those whose lung tumors retained chromosome 3p24 (Supp Fig. 5E).

DISCUSSION

Transposon-mediated mutagenesis has played a prominent role in the genetic analysis of normal development, physiology and of various diseases, especially in models of human cancer (53,54). Indeed, the initial identification of c-MYC and WNT1 as oncogenes came from analysis of lymphoma in chickens and mammary neoplasias in mice respectively (55–57). More recently, the resurrection of the TC1/Mariner-based *Sleeping Beauty* transposase in conjunction with engineered *T2/Onc* transposable elements in both mice or zebrafish have served to identify numerous tumor suppressors and/or oncogenes involved in cancer initiation, progression or maintenance (16,21,22,26,27,58–64).

Here, we describe the use of transposon mutagenesis to identify genes that cooperate to promote progression of BRAF^{V600E}-driven benign adenomas to malignant lung cancers. While this screen was not saturating, since known suppressors of BRAF^{V600E}-driven lung cancer such as *Trp53*, *Pten* or *Cdkn2a* were not identified, it was advantageous in that we identified a number of new cooperating genes including: *Rbms3*, *Foxp1*, *Arid1b*, *Snd1*, *Gnaq* and *Cux1*. Some of these have previously been shown to play a role in cancer: 1. SB-mediated *Cux1* inactivation was reported to promote progression of myeloid malignancies (65); 2. *GNAQ*, the human ortholog of *Gnaq*, is a noted human oncogene mutated in uveal melanoma (66); 3. *Foxp1* encodes a transcriptional regulator of lung endoderm development, but is reported to contribute to various cancers (67,68); and 4. *SND1* has been found fused to *BRAF* to form an oncogenic fusion gene in never smoker lung adenocarcinoma (69). Hence, our SB screen collectively identified a number of genes implicated in neoplastic transformation.

The mechanistic role of *RBMS3* in normal development, physiology or cancer remains largely obscure, but previous work has shed light on select aspects of its potential biological roles (70). The protein contains two pairs of RNA binding motifs and is related to members of the c-MYC single-strand binding proteins (MSSPs) that are thought to regulate DNA replication, transcription, apoptosis and cell cycle progression by interacting with c-MYC (35). Here, we shown that *RBMS3* silencing, in combination with either the BRAF^{V600E} or the EGFR^{L858R} oncoproteins, can promote lung carcinogenesis. The precise mechanism of cooperation remains uncertain but given its reported ability to regulate signaling through the WNT> β -catenin>c-MYC, a pathway essential for KRAS^{G12D}- or BRAF^{V600E}-driven lung cancer, this seems like a likely mechanism (35–37,41). Moreover, other studies

have suggested a role for RBMS3 as a suppressor of breast, esophageal, ovarian, gastric cancer, and lung squamous cell carcinoma (36–42). Interestingly, *RBMS3* is located on chromosome 3 in a region that undergoes copy number loss in a substantial number of lung cancer patients. Taken together, this data provides a compelling rationale for developing a deeper mechanistic understanding of the biochemical mechanisms of RBMS3 tumor suppression, and how loss of such cooperates with common lung cancer oncoprotein kinases such as BRAF^{V600E} and EGFR^{L858R}.

Numerous and diverse approaches have demonstrated that WNT signaling is critical in normal lung development, physiology, and in the progression and/or maintenance of lung cancer (14,43–46). These data not only emphasize the importance of this pathway in lung cancer, but brings about a critical question, begging whether all roads eventually lead to WNT signaling as a major player regulating lung cancer progression? We have previously shown that WNT> β -catenin signaling is essential for BRAF^{V600E}-induced benign lung tumorigenesis. Moreover, diminished WNT signaling serves as a barrier to the malignant progression of BRAF^{V600E}-induced benign adenomas (14). Mechanistically, BRAF^{V600E} plus WNT> β -catenin signaling cooperatively converge to promote expression of c-MYC. Moreover, WNT signaling is also reported to be essential for growth of KRAS^{G12D}/TP53^{Null} GEM lung cancers (45). Here, RBMS3 silencing led to elevated expression of β -Catenin, Axin2, Lgr5, c-Myc and Cyclin D1 mRNAs in lung tumors, indicating that silencing of the pathway is promoting transcription of relevant WNT target genes. Interestingly, BRAF^{V600E}/RBMS3^{Null} lung tumors remained sensitive to LGK974, a potent and specific inhibitor of Porcupine (PRCN), the enzyme essential for post-translational acylation and secretion of most WNT ligands (71,72). Our work also revealed that RBMS3 silencing led to resistance of BRAF^{V600E}-driven lung tumors to pathway-targeted inhibition of BRAF^{V600E} signaling. RBMS3 has been implicated in the regulation of *TWIST1* expression in metastatic breast cancer, by directly binding to the 3'-UTR of Twist1 mRNA (42). Finally, given the ability of RBMS3 silencing to elicit drug resistance in BRAF^{V600E}-driven lung tumors, it would be interesting in the future to test whether the same is true in lung cancers driven by mutationally-activated EGFR, which could have clinical implications for the treatment of this set of patients.

In summary, using a variety of technique starting with SB-mediated transposon mutagenesis, we revealed RBMS3 to be a suppressor of lung tumorigenesis driven by the BRAF^{V600E} or EGFR^{L858R} oncoprotein kinases. Interestingly, *RBMS3* is located on a region of chromosome 3 that is subject to copy number loss in a significant number of lung cancer patients.

Supplementary Material

Refer to Web version on PubMed Central for supplementary material.

ACKNOWLEDGEMENTS

The authors have made a good-faith effort to appropriately acknowledge everyone who contributed to this project over the past 12 years. The authors thank Dr. Shin-Heng Chiou from Dr. Monte Winslow's lab at Stanford University for technical advice and assistance in preparing reagents and executing experiments for these studies,

and Dr. Winslow himself for graciously sharing the *H1^{LSL}-CAS9* mice with us. The authors thank Dr. Rachele Olsen and Dr. Gurkan Mollaoglu from Dr. Trudy Oliver's lab at the Huntsman Cancer Institute for their assistance in providing control samples and troubleshooting for certain experiments. The authors thank Dr. Eric Snyder and the members of his lab, especially Dr. Soledad Camolotto and Katy Gillis, for technical expertise and assistance supporting these studies. We particularly acknowledge and thank Dr. Harold Varmus for graciously providing key mouse strains from his laboratory in advance of their publication. The authors thank the staff of the following University of Utah or HCI Shared Resources for advice, guidance and technical support: 1. High Throughput Genomics; 2. Flow Cytometry and; 3. Biorepository and Molecular Pathology Shared Resources (Supported by CA042014). Financial support for this publication was supported by the NCI R01_CA131261 to MM, F32CA228267 and K99CA246084 to AV, Cancer Research UK 21717 to DA, as well as a Genentech Foundation Graduate Fellowship Award to JJ.

REFERENCES

1. Siegel RL, Miller KD, Jemal A. Cancer statistics, 2016. *CA Cancer J Clin* 2016;66:7–30 [PubMed: 26742998]
2. Drilon A, Laetsch TW, Kummar S, DuBois SG, Lassen UN, Demetri GD, et al. Efficacy of Larotrectinib in TRK Fusion-Positive Cancers in Adults and Children. *N Engl J Med* 2018;378:731–9 [PubMed: 29466156]
3. Soria JC, Ohe Y, Vansteenkiste J, Reungwetwattana T, Chewaskulyong B, Lee KH, et al. Osimertinib in Untreated EGFR-Mutated Advanced Non-Small-Cell Lung Cancer. *N Engl J Med* 2018;378:113–25 [PubMed: 29151359]
4. Peters S, Camidge DR, Shaw AT, Gadgeel S, Ahn JS, Kim DW, et al. Alectinib versus Crizotinib in Untreated ALK-Positive Non-Small-Cell Lung Cancer. *N Engl J Med* 2017;377:829–38 [PubMed: 28586279]
5. Vultur A, Herlyn M. SnapShot: melanoma. *Cancer Cell* 2013;23:706–e1 [PubMed: 23680152]
6. Heist RS, Engelman JA. SnapShot: non-small cell lung cancer. *Cancer Cell* 2012;21:448 e2
7. Holderfield M, Deuker MM, McCormick F, McMahon M. Targeting RAF kinases for cancer therapy: BRAF-mutated melanoma and beyond. *Nature reviews Cancer* 2014;14:455–67 [PubMed: 24957944]
8. Cancer Genome Atlas Research N. Comprehensive molecular profiling of lung adenocarcinoma. *Nature* 2014;511:543–50 [PubMed: 25079552]
9. Planchard D, Smit EF, Groen HJM, Mazieres J, Besse B, Helland A, et al. Dabrafenib plus trametinib in patients with previously untreated BRAF(V600E)-mutant metastatic non-small-cell lung cancer: an open-label, phase 2 trial. *Lancet Oncol* 2017;18:1307–16 [PubMed: 28919011]
10. Dummer R, Ascierto PA, Gogas HJ, Arance A, Mandala M, Liskay G, et al. Encorafenib plus binimetinib versus vemurafenib or encorafenib in patients with BRAF-mutant melanoma (COLUMBUS): a multicentre, open-label, randomised phase 3 trial. *Lancet Oncol* 2018;19:603–15 [PubMed: 29573941]
11. Larkin J, Ascierto PA, Dreno B, Atkinson V, Liskay G, Maio M, et al. Combined vemurafenib and cobimetinib in BRAF-mutated melanoma. *N Engl J Med* 2014;371:1867–76 [PubMed: 25265494]
12. Dankort D, Filenova E, Collado M, Serrano M, Jones K, McMahon M. A new mouse model to explore the initiation, progression, and therapy of BRAFV600E-induced lung tumors. *Genes Dev* 2007;21:379–84 [PubMed: 17299132]
13. van Veen JE, Scherzer M, Boshuizen J, Chu M, Liu A, Landman A, et al. Mutationally-activated PI3'-kinase-alpha promotes de-differentiation of lung tumors initiated by the BRAF(V600E) oncoprotein kinase. *Elife* 2019;8
14. Juan J, Muraguchi T, Iezza G, Sears RC, McMahon M. Diminished WNT -> beta-catenin -> c-MYC signaling is a barrier for malignant progression of BRAFV600E-induced lung tumors. *Genes Dev* 2014;28:561–75 [PubMed: 24589553]
15. Trejo CL, Green S, Marsh V, Collisson EA, Iezza G, Phillips WA, et al. Mutationally activated PIK3CA(H1047R) cooperates with BRAF(V600E) to promote lung cancer progression. *Cancer Res* 2013;73:6448–61 [PubMed: 24019382]
16. Mann MB, Black MA, Jones DJ, Ward JM, Yew CC, Newberg JY, et al. Transposon mutagenesis identifies genetic drivers of Braf(V600E) melanoma. *Nat Genet* 2015;47:486–95 [PubMed: 25848750]

17. Montero-Conde C, Leandro-Garcia LJ, Chen X, Oler G, Ruiz-Llorente S, Ryder M, et al. Transposon mutagenesis identifies chromatin modifiers cooperating with Ras in thyroid tumorigenesis and detects ATXN7 as a cancer gene. *Proc Natl Acad Sci U S A* 2017;114:E4951–E60 [PubMed: 28584132]
18. Weber J, Braun CJ, Saur D, Rad R. In vivo functional screening for systems-level integrative cancer genomics. *Nature reviews Cancer* 2020;20:573–93 [PubMed: 32636489]
19. de la Rosa J, Weber J, Friedrich MJ, Li Y, Rad L, Ponstingl H, et al. A single-copy Sleeping Beauty transposon mutagenesis screen identifies new PTEN-cooperating tumor suppressor genes. *Nature genetics* 2017;49:730–41 [PubMed: 28319090]
20. Uren AG, Mikkers H, Kool J, van der Weyden L, Lund AH, Wilson CH, et al. A high-throughput splinkerette-PCR method for the isolation and sequencing of retroviral insertion sites. *Nat Protoc* 2009;4:789–98 [PubMed: 19528954]
21. Brett BT, Berquam-Vrieze KE, Nannapaneni K, Huang J, Scheetz TE, Dupuy AJ. Novel molecular and computational methods improve the accuracy of insertion site analysis in Sleeping Beauty-induced tumors. *PLoS One* 2011;6:e24668 [PubMed: 21931803]
22. Takeda H, Rust AG, Ward JM, Yew CC, Jenkins NA, Copeland NG. Sleeping Beauty transposon mutagenesis identifies genes that cooperate with mutant Smad4 in gastric cancer development. *Proc Natl Acad Sci U S A* 2016;113:E2057–65 [PubMed: 27006499]
23. Chiou SH, Winters IP, Wang J, Naranjo S, Dudgeon C, Tamburini FB, et al. Pancreatic cancer modeling using retrograde viral vector delivery and in vivo CRISPR/Cas9-mediated somatic genome editing. *Genes Dev* 2015;29:1576–85 [PubMed: 26178787]
24. Ullman-Cullere MH, Foltz CJ. Body condition scoring: a rapid and accurate method for assessing health status in mice. *Lab Anim Sci* 1999;49:319–23 [PubMed: 10403450]
25. DuPage M, Dooley AL, Jacks T. Conditional mouse lung cancer models using adenoviral or lentiviral delivery of Cre recombinase. *Nat Protoc* 2009;4:1064–72 [PubMed: 19561589]
26. Collier LS, Carlson CM, Ravimohan S, Dupuy AJ, Largaespada DA. Cancer gene discovery in solid tumours using transposon-based somatic mutagenesis in the mouse. *Nature* 2005;436:272–6 [PubMed: 16015333]
27. Dupuy AJ, Akagi K, Largaespada DA, Copeland NG, Jenkins NA. Mammalian mutagenesis using a highly mobile somatic Sleeping Beauty transposon system. *Nature* 2005;436:221–6 [PubMed: 16015321]
28. Boj SF, Hwang CI, Baker LA, Chio II, Engle DD, Corbo V, et al. Organoid models of human and mouse ductal pancreatic cancer. *Cell* 2015;160:324–38 [PubMed: 25557080]
29. Zewdu R, Mehrabad EM, Ingram K, Fang P, Gillis KL, Camolotto SA, et al. An NKX2–1/ERK/WNT feedback loop modulates gastric identity and response to targeted therapy in lung adenocarcinoma. *Elife* 2021;10
30. Miyoshi H, Stappenbeck TS. In vitro expansion and genetic modification of gastrointestinal stem cells in spheroid culture. *Nat Protoc* 2013;8:2471–82 [PubMed: 24232249]
31. Vaishnavi A, Schubert L, Rix U, Marek LA, Le AT, Keysar SB, et al. EGFR Mediates Responses to Small-Molecule Drugs Targeting Oncogenic Fusion Kinases. *Cancer Res* 2017;77:3551–63 [PubMed: 28428274]
32. Mollaoglu G, Guthrie MR, Bohm S, Bragelmann J, Can I, Ballieu PM, et al. MYC Drives Progression of Small Cell Lung Cancer to a Variant Neuroendocrine Subtype with Vulnerability to Aurora Kinase Inhibition. *Cancer Cell* 2017;31:270–85 [PubMed: 28089889]
33. Camolotto SA, Pattabiraman S, Mosbrugger TL, Jones A, Belova VK, Orstad G, et al. FoxA1 and FoxA2 drive gastric differentiation and suppress squamous identity in NKX2–1-negative lung cancer. *Elife* 2018;7
34. Su Q, Prosser HM, Campos LS, Ortiz M, Nakamura T, Warren M, et al. A DNA transposon-based approach to validate oncogenic mutations in the mouse. *Proc Natl Acad Sci U S A* 2008;105:19904–9 [PubMed: 19064922]
35. Penkov D, Ni R, Else C, Pinol-Roma S, Ramirez F, Tanaka S. Cloning of a human gene closely related to the genes coding for the c-myc single-strand binding proteins. *Gene* 2000;243:27–36 [PubMed: 10675610]

36. Wu Y, Yun D, Zhao Y, Wang Y, Sun R, Yan Q, et al. Down regulation of RNA binding motif, single-stranded interacting protein 3, along with up regulation of nuclear HIF1A correlates with poor prognosis in patients with gastric cancer. *Oncotarget* 2017;8:1262–77 [PubMed: 27902480]
37. Li Y, Chen L, Nie CJ, Zeng TT, Liu H, Mao X, et al. Downregulation of RBMS3 is associated with poor prognosis in esophageal squamous cell carcinoma. *Cancer Res* 2011;71:6106–15 [PubMed: 21844183]
38. Wu G, Cao L, Zhu J, Tan Z, Tang M, Li Z, et al. Loss of RBMS3 Confers Platinum Resistance in Epithelial Ovarian Cancer via Activation of miR-126–5p/beta-catenin/CBP signaling. *Clin Cancer Res* 2019;25:1022–35 [PubMed: 30279231]
39. Chen J, Kwong DL, Zhu CL, Chen LL, Dong SS, Zhang LY, et al. RBMS3 at 3p24 inhibits nasopharyngeal carcinoma development via inhibiting cell proliferation, angiogenesis, and inducing apoptosis. *PLoS One* 2012;7:e44636 [PubMed: 22957092]
40. Yang Y, Quan L, Ling Y. RBMS3 Inhibits the Proliferation and Metastasis of Breast Cancer Cells. *Oncol Res* 2017
41. Liang YN, Liu Y, Meng Q, Li X, Wang F, Yao G, et al. RBMS3 is a tumor suppressor gene that acts as a favorable prognostic marker in lung squamous cell carcinoma. *Med Oncol* 2015;32:459 [PubMed: 25588924]
42. Zhu L, Xi PW, Li XX, Sun X, Zhou WB, Xia TS, et al. The RNA binding protein RBMS3 inhibits the metastasis of breast cancer by regulating Twist1 expression. *J Exp Clin Cancer Res* 2019;38:105
43. Nabhan AN, Brownfield DG, Harbury PB, Krasnow MA, Desai TJ. Single-cell Wnt signaling niches maintain stemness of alveolar type 2 cells. *Science* 2018;359:1118–23 [PubMed: 29420258]
44. Kadzik RS, Cohen ED, Morley MP, Stewart KM, Lu MM, Morrisey EE. Wnt ligand/Frizzled 2 receptor signaling regulates tube shape and branch-point formation in the lung through control of epithelial cell shape. *Proc Natl Acad Sci U S A* 2014;111:12444–9 [PubMed: 25114215]
45. Tammela T, Sanchez-Rivera FJ, Cetinbas NM, Wu K, Joshi NS, Helenius K, et al. A Wnt-producing niche drives proliferative potential and progression in lung adenocarcinoma. *Nature* 2017;545:355–9 [PubMed: 28489818]
46. Desai TJ, Brownfield DG, Krasnow MA. Alveolar progenitor and stem cells in lung development, renewal and cancer. *Nature* 2014;507:190–4 [PubMed: 24499815]
47. De Oliveira Duarte Achcar R, Nikiforova MN, Yousem SA. Micropapillary lung adenocarcinoma: EGFR, K-ras, and BRAF mutational profile. *American journal of clinical pathology* 2009;131:694–700 [PubMed: 19369630]
48. Fatehullah A, Tan SH, Barker N. Organoids as an in vitro model of human development and disease. *Nat Cell Biol* 2016;18:246–54 [PubMed: 26911908]
49. Rock JR, Onaitis MW, Rawlins EL, Lu Y, Clark CP, Xue Y, et al. Basal cells as stem cells of the mouse trachea and human airway epithelium. *Proc Natl Acad Sci U S A* 2009;106:12771–5 [PubMed: 19625615]
50. Politi K, Zakowski MF, Fan PD, Schonfeld EA, Pao W, Varmus HE. Lung adenocarcinomas induced in mice by mutant EGF receptors found in human lung cancers respond to a tyrosine kinase inhibitor or to down-regulation of the receptors. *Genes Dev* 2006;20:1496–510 [PubMed: 16705038]
51. Cerami E, Gao J, Dogrusoz U, Gross BE, Sumer SO, Aksoy BA, et al. The cBio cancer genomics portal: an open platform for exploring multidimensional cancer genomics data. *Cancer Discov* 2012;2:401–4 [PubMed: 22588877]
52. Gao J, Aksoy BA, Dogrusoz U, Dresdner G, Gross B, Sumer SO, et al. Integrative analysis of complex cancer genomics and clinical profiles using the cBioPortal. *Sci Signal* 2013;6:pl1
53. Wieschaus E, Nusslein-Volhard C. The Heidelberg Screen for Pattern Mutants of *Drosophila*: A Personal Account. *Annu Rev Cell Dev Biol* 2016;32:1–46 [PubMed: 27501451]
54. Cain AK, Barquist L, Goodman AL, Paulsen IT, Parkhill J, van Opijnen T. A decade of advances in transposon-insertion sequencing. *Nat Rev Genet* 2020;21:526–40 [PubMed: 32533119]
55. Hayward WS, Neel BG, Astrin SM. Activation of a cellular onc gene by promoter insertion in ALV-induced lymphoid leukemia. *Nature* 1981;290:475–80 [PubMed: 6261142]

56. Neel BG, Hayward WS, Robinson HL, Fang J, Astrin SM. Avian leukosis virus-induced tumors have common proviral integration sites and synthesize discrete new RNAs: oncogenesis by promoter insertion. *Cell* 1981;23:323–34 [PubMed: 6258798]
57. Nusse R, Varmus HE. Many tumors induced by the mouse mammary tumor virus contain a provirus integrated in the same region of the host genome. *Cell* 1982;31:99–109 [PubMed: 6297757]
58. Copeland NG, Jenkins NA. Harnessing transposons for cancer gene discovery. *Nature reviews Cancer* 2010;10:696–706 [PubMed: 20844553]
59. Mann KM, Ward JM, Yew CC, Kovochich A, Dawson DW, Black MA, et al. Sleeping Beauty mutagenesis reveals cooperating mutations and pathways in pancreatic adenocarcinoma. *Proc Natl Acad Sci U S A* 2012;109:5934–41 [PubMed: 22421440]
60. Collier LS, Adams DJ, Hackett CS, Bendzick LE, Akagi K, Davies MN, et al. Whole-body sleeping beauty mutagenesis can cause penetrant leukemia/lymphoma and rare high-grade glioma without associated embryonic lethality. *Cancer Res* 2009;69:8429–37 [PubMed: 19843846]
61. To JC, Chiu AP, Tschida BR, Lo LH, Chiu CH, Li XX, et al. ZBTB20 regulates WNT/CTNNB1 signalling pathway by suppressing PPARG during hepatocellular carcinoma tumorigenesis. *JHEP Rep* 2021;3:100223
62. Beckmann PJ, Larson JD, Larsson AT, Ostergaard JP, Wagner S, Rahrman EP, et al. Sleeping Beauty Insertional Mutagenesis Reveals Important Genetic Drivers of Central Nervous System Embryonal Tumors. *Cancer Res* 2019;79:905–17 [PubMed: 30674530]
63. Rahrman EP, Wolf NK, Otto GM, Heltemes-Harris L, Ramsey LB, Shu J, et al. Sleeping Beauty Screen Identifies RREB1 and Other Genetic Drivers in Human B-cell Lymphoma. *Molecular cancer research : MCR* 2019;17:567–82 [PubMed: 30355676]
64. McGrail M, Hatler JM, Kuang X, Liao HK, Nannapaneni K, Watt KE, et al. Somatic mutagenesis with a Sleeping Beauty transposon system leads to solid tumor formation in zebrafish. *PLoS One* 2011;6:e18826 [PubMed: 21533036]
65. Wong CC, Martincorena I, Rust AG, Rashid M, Alifrangis C, Alexandrov LB, et al. Inactivating CUX1 mutations promote tumorigenesis. *Nature genetics* 2014;46:33–8 [PubMed: 24316979]
66. Truong A, Yoo JH, Scherzer MT, Sanchez JMS, Dale KJ, Kinsey CG, et al. Chloroquine Sensitizes GNAQ11-mutated Melanoma to MEK1/2 Inhibition. *Clin Cancer Res* 2020;26:6374–86 [PubMed: 32933997]
67. Li S, Morley M, Lu M, Zhou S, Stewart K, French CA, et al. Foxp transcription factors suppress a non-pulmonary gene expression program to permit proper lung development. *Dev Biol* 2016;416:338–46 [PubMed: 27341756]
68. Koon HB, Ippolito GC, Banham AH, Tucker PW. FOXP1: a potential therapeutic target in cancer. *Expert Opin Ther Targets* 2007;11:955–65 [PubMed: 17614763]
69. Jang JS, Lee A, Li J, Liyanage H, Yang Y, Guo L, et al. Common Oncogene Mutations and Novel SND1-BRAF Transcript Fusion in Lung Adenocarcinoma from Never Smokers. *Sci Rep* 2015;5:9755 [PubMed: 25985019]
70. Jayasena CS, Bronner ME. Rbms3 functions in craniofacial development by posttranscriptionally modulating TGF-beta signaling. *The Journal of cell biology* 2012;199:453–66 [PubMed: 23091072]
71. Jiang X, Hao HX, Growney JD, Woolfenden S, Bottiglio C, Ng N, et al. Inactivating mutations of RNF43 confer Wnt dependency in pancreatic ductal adenocarcinoma. *Proc Natl Acad Sci U S A* 2013;110:12649–54 [PubMed: 23847203]
72. Lum L, Clevers H. Cell biology. The unusual case of Porcupine. *Science* 2012;337:922–3 [PubMed: 22923569]

SIGNIFICANCE

Loss of RBMS3 cooperates with BRAF^{V600E} to induce lung tumorigenesis, providing a deeper understanding of the molecular mechanisms underlying mutant BRAF-driven lung cancer and potential strategies to more effectively target this disease.

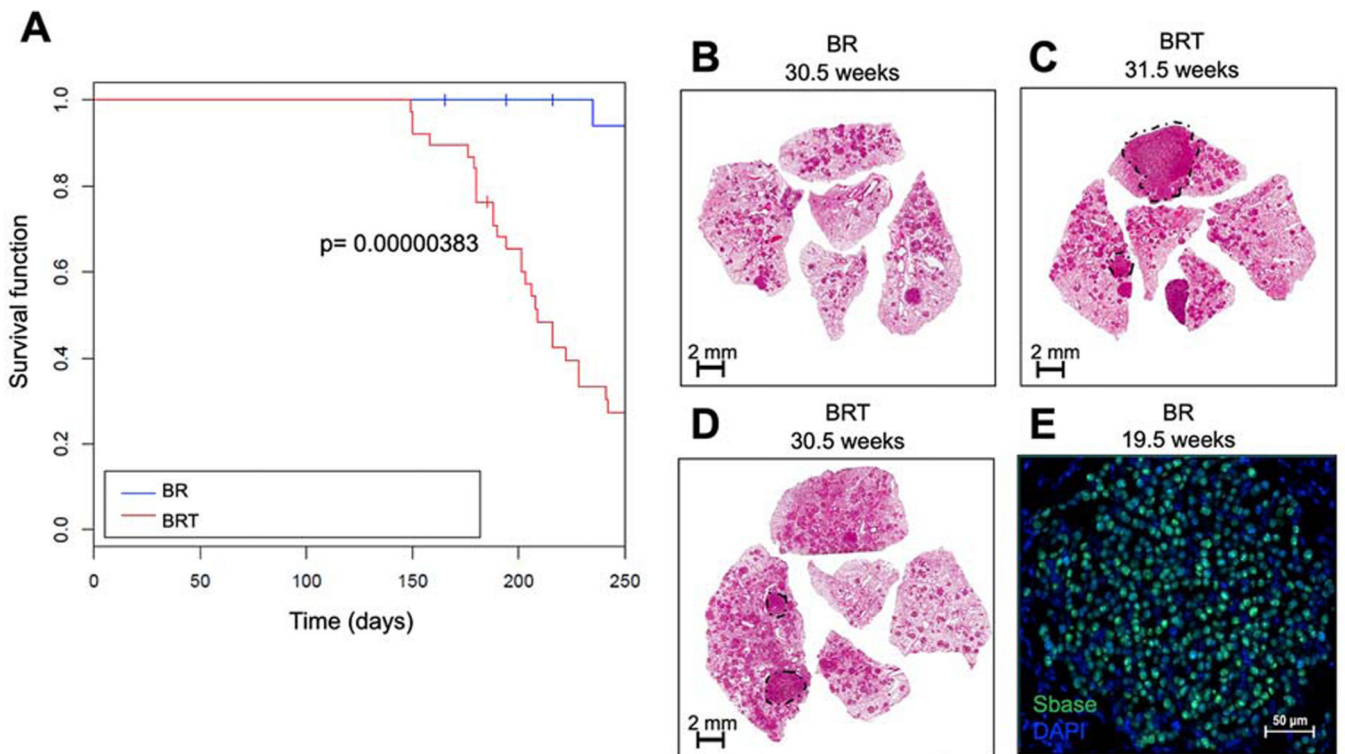


Figure 1. The Sleeping Beauty (SB) transposon system promotes lethal malignant progression of BRAF^{V600E}-driven lung tumors in a GEM model.

A: Kaplan Meier survival curve tracking survival of 50 *Braf*^{CA} and SB (CAGG/*R26*^{L^{SL}-SB11}) or (*BR*) mice, either with or without a *T2/Onc2* transposon or (*BRT*) mice donor on chromosome 4 (*C4*^{T2/Onc2}) for 250 days. Mice were initiated through intranasal instillation with 10⁶ pfu of Ad5.CMV-CRE. Statistical analysis was performed using a log-rank Mantel-Cox test where $p = 0.00000383$. **B-D:** Histological analyses of formalin fixed paraffin embedded (FFPE) tumor bearing lung sections stained with hematoxylin and eosin (H&E). **E:** Expression of SB transposase in *BR* mouse lung tumors at 19.5 weeks post-initiation assessed by immunofluorescence analysis of FFPE sections of mouse lungs. DAPI stained DNA is blue and SB11 Transposase is in green.

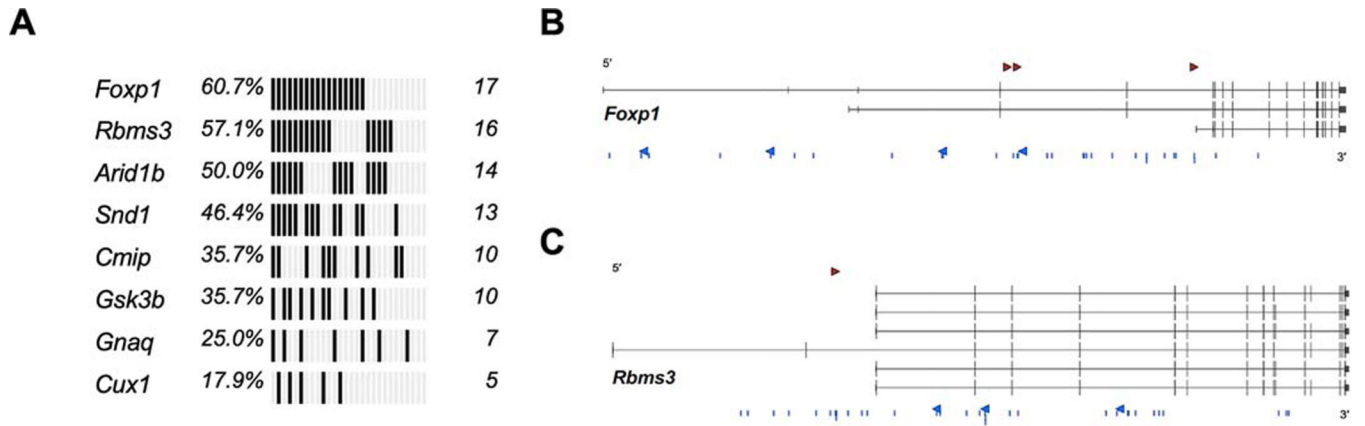


Figure 2. Genomic landscape of *SB/Braf* lung drivers.

A: Oncoprint of statistically significant drivers in BRAF^{V600E}-driven lung tumors detected using GKC analysis, using SB common integration regions (CIRs), and Truncal SB Driver Analysis, using unique, directional SB insertions at TA-dinucleotides. **B:** SB insertions at TA-dinucleotides with sense (red arrowhead) and anti-sense (blue arrowheads) and within CIRs (blue lines) for *Foxp1* (3 transcripts of the genes are shown). **C:** SB insertions at TA-dinucleotides with sense (red arrowhead) and anti-sense (blue arrowheads) and within CIRs (blue lines) for *Rbms3* (6 transcripts of the candidate gene are shown).

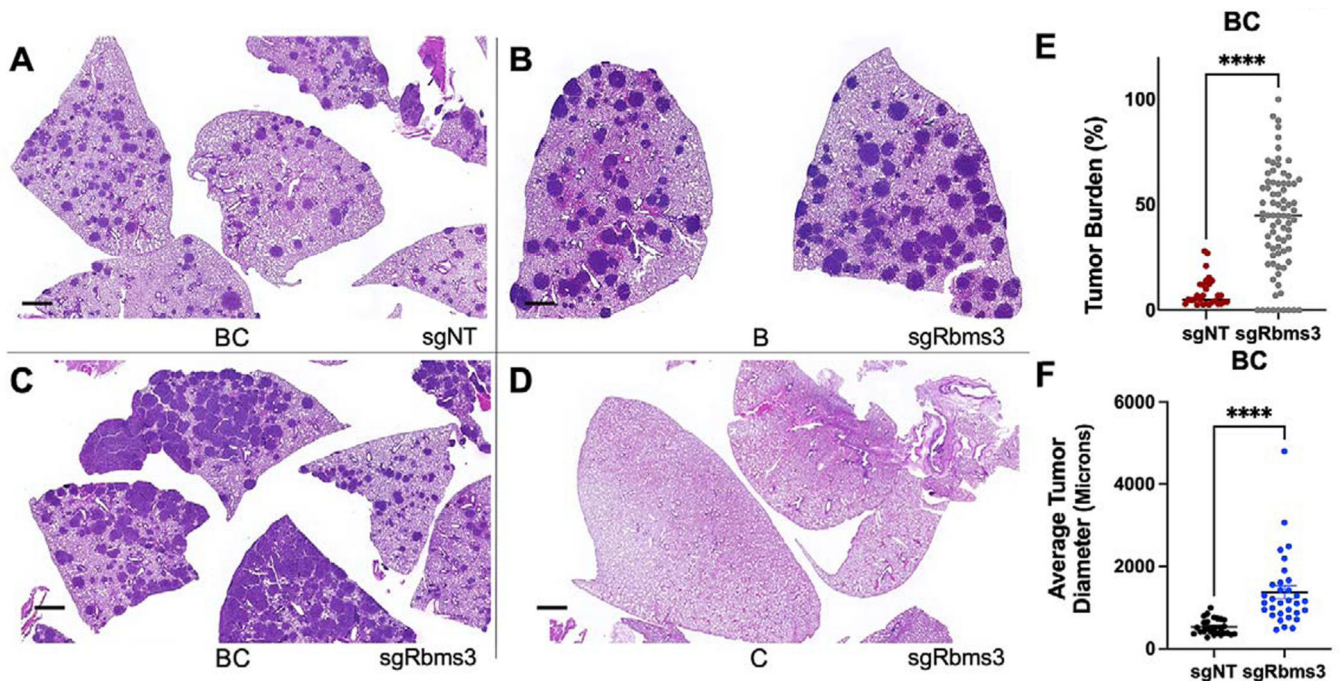


Figure 3. CRISPR/Cas9 editing of *Rbms3* cooperates with BRAF^{V600E} in a mouse model of lung cancer.

A-D: Representative images of different genotypes of harvested mouse lung sections following necropsy analyses stained with hematoxylin and eosin (H&E) 13 weeks post initiation with 5×10^4 pfu lenti-CRE. CRISPR/CAS9-mediated genome editing was used in panels **A**, **C**, **D** to edit *Rbms3* *in vivo*. Genotype and average tumor burden calculation of each experimental group was: **A:** sgNT-CRE virus in *Braf*^{CAT/+}; *H11*^{LSL-CAS9} (*BC*) mice: **8.5%**. **B:** sgRbms3-CRE virus in *Braf*^{CAT/+} (*B*) mice: **7.7%**. **C:** sgRbms3-CRE virus in *BC* mice: **38.8%**. **D:** sgRbms3-CRE virus in *H11*^{LSL-CAS9/+} (*C*) mice: **0%**. Black bar in bottom left of each panel represents a 1000-micron scale bar. **E:** Quantification of individual tumor burden from genotypes in panel **A** compared to panel **C**. Tumor bearing lungs from panel **B** were identical to panel **A**. A paired T-test was used to determine statistical significance; $p < 0.01$. **F:** Quantification of tumor diameter was performed in microns using 25 individual tumors from genotypes in panel **A** compared to panel **C** using the 3D Histech MIDI Slide Scanner QuantCenter. Comprehensive analyses was conducted with over 200 lung tumors. $N=50$ mice individual or (biological replicates). $N = 2$ experimental replicates were performed comparing the indicated genotypes in **A** and **C**. Individual values are graphed, the black bar represents the mean, and the error bars represent SEM. A paired T-test was used to determine statistical significance; $p < 0.0001$.

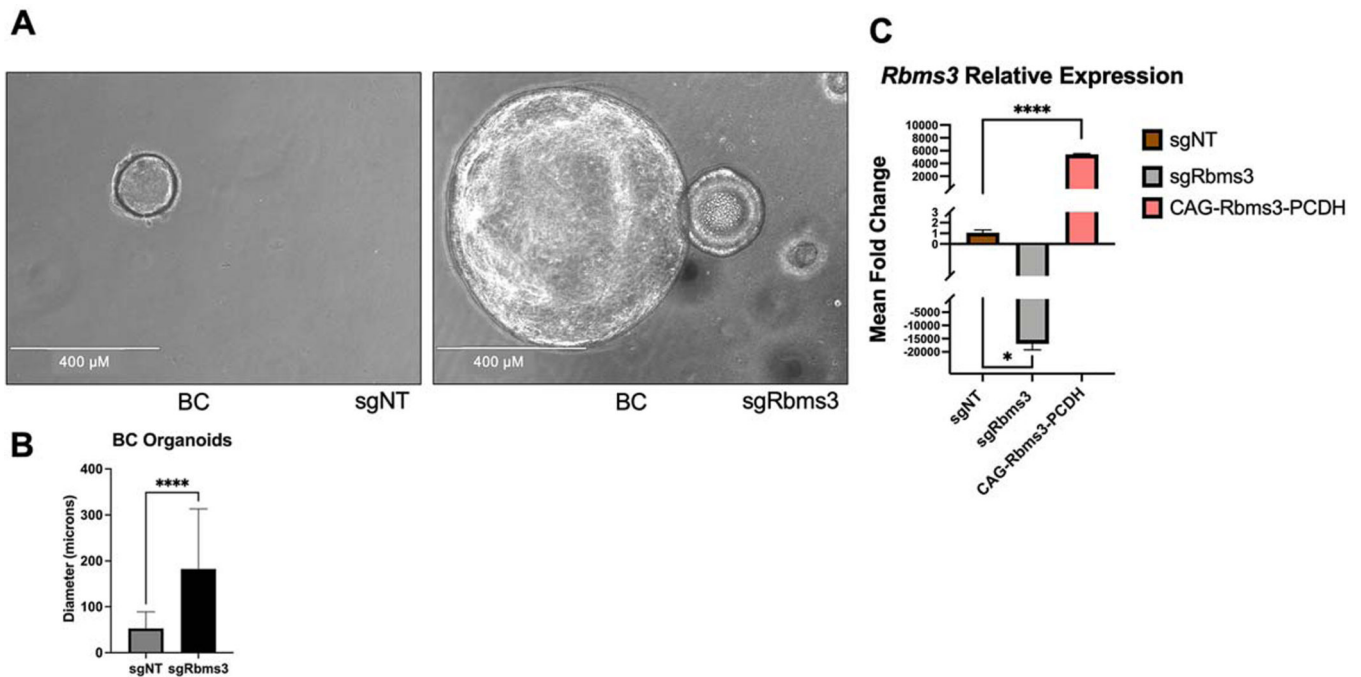


Figure 4. *Rbms3* silencing cooperates with BRAF^{V600E} to promote the growth of lung organoids.

A: Representative images are shown of qualitative analyses of phase contrast images of organoids established following tumor dissociation from *BC* mice at 7 days post-initiation of organoids. White scale bar indicates 400 microns, and was taken with 10x magnification. N=12 technical replicates with 3 biological replicates leveraging pooled lung lobes from N=8 mice. **B:** Quantification of organoid diameters at 7 days post-initiation of organoids from lungs of the indicated mouse genotypes described in (A). **C:** qRT-PCR analysis of *Rbms3* mRNA expression in organoids derived from *BC* mice labeled by the lentivirus they were initiated with. Transient over-expression of wild-type *Rbms3* was used as a positive control for gene expression. Mean is graphed and error bars represent SEM. Statistical analysis was conducted using a paired T test; * = $p < 0.05$; **** = $p < 0.0001$.

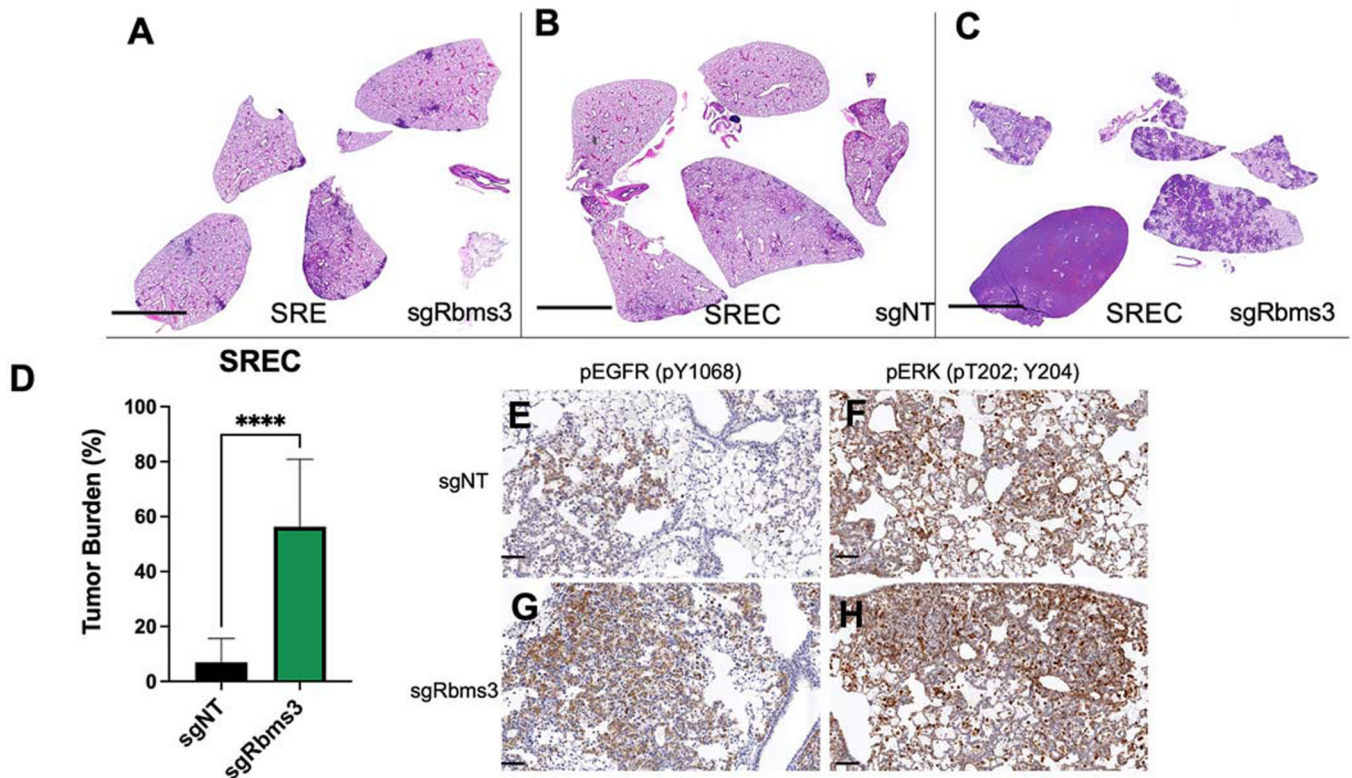


Figure 5. *Rbms3* loss cooperates with *EGFR*^{L858R} to accelerate malignant lung adenocarcinoma

A-C: Images of harvested mouse lung sections following necropsy analyses stained with hematoxylin and eosin (H&E) 11 weeks post initiation with 1×10^5 pfu lenti-CRE, followed by continuous administration of doxycycline chow to induce *EGFR*^{L858R} expression. CRISPR/CAS9-mediated genome editing was used in panels **B** and **C** to edit *Rbms3* *in vivo*. Genotype of each experimental group was: **A:** sgRbms3-CRE virus in *SPC::CRE-ERT2/+; Rosa26^{CAGs-LSL-rTTa3}; EGFR^{L858R}* (*SRE*) mice. **B:** sgNT-CRE virus in or *SPC::CRE-ERT2/+; Rosa26^{CAGs-LSL-rTTa3}; EGFR^{L858R}; H1^{LSL-CAS9/+}* (*SREC*) mice. **C:** sgRbms3-CRE virus in *SREC* mice. Black bar in bottom left of each panel represents a 1000-micron scale bar. **D:** Quantification of tumor burden from genotypes in panel **B** compared to panel **C**. N=5 mice per group. The mean is graphed, and error bars represent SEM. Statistical analysis was conducted using a paired T test; **** = p < 0.0001. **E:** Representative images of immunohistochemistry on FFPE lung tissue sections from *SREC* mice initiated with either sgNT- or sgRbms3-CRE and stained with pEGFR (pY1068) or pERK (pT202; Y204) shown at 20x magnification. Scale bar shown in black at the bottom left corner of each image represent 50 microns.

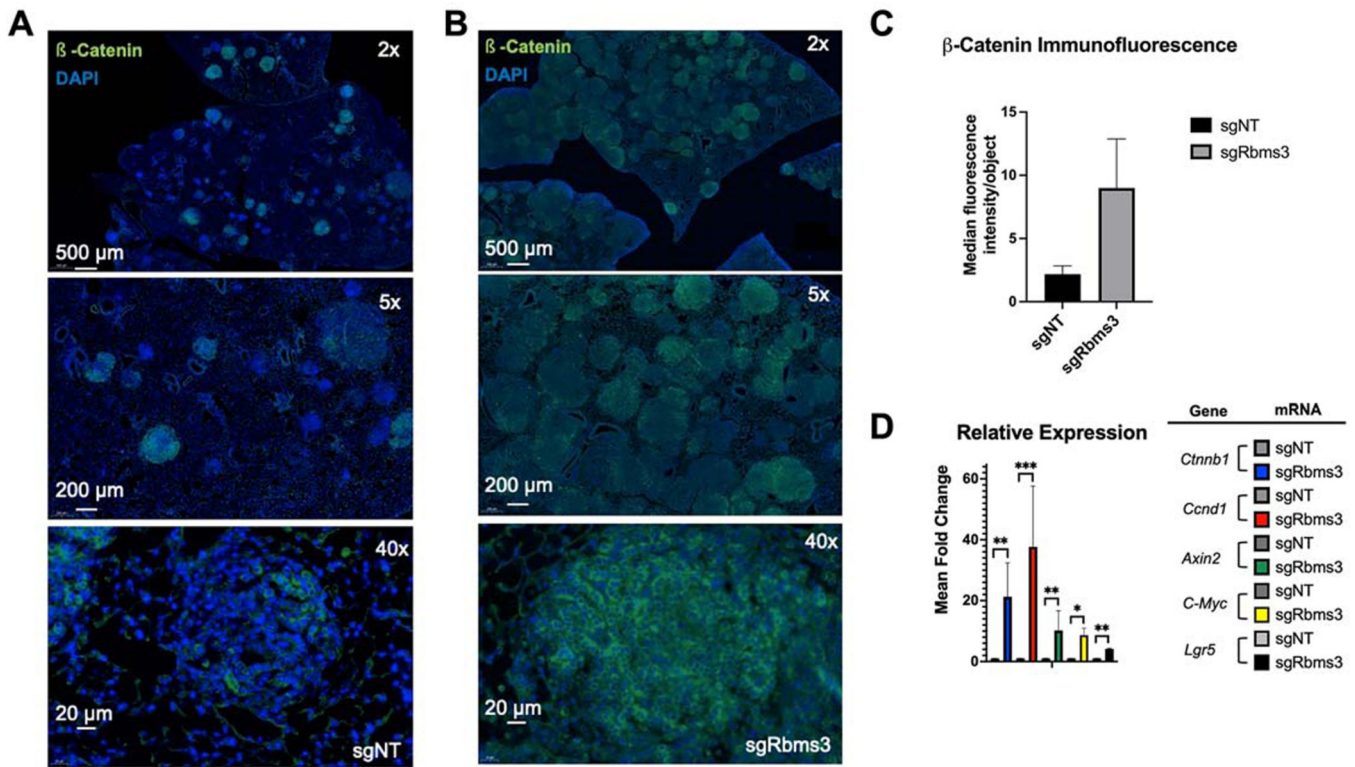


Figure 6. WNT signaling components are expressed at higher levels in BC lung tumors without *Rbms3*.

A&B: Representative images of β -catenin expression as assessed by indirect immunofluorescent in tumor bearing FFPE BC mouse lung sections (shown at 2x, 5x, and 40 magnifications) initiated with either **A:** sgNT-CRE or **B:** sgRbms3-CRE. Scale bars are shown in white in the bottom left corner of each image as indicated. **C:** Median fluorescence intensity quantitation using cellprofiler software. **D:** qRT-PCR analysis of BC organoids from the indicated viral initiation groups using probes to detect *Ctnnb1*, *Ccnd1*, *Axin2*, *Lgr5*, or *c-Myc* mRNAs. Mean is graphed with error bars as SEM. Statistical analysis was conducted using a paired T test; * = $p < 0.05$; ** = $p < 0.01$; *** = $p < 0.001$; **** = $p < 0.0001$.

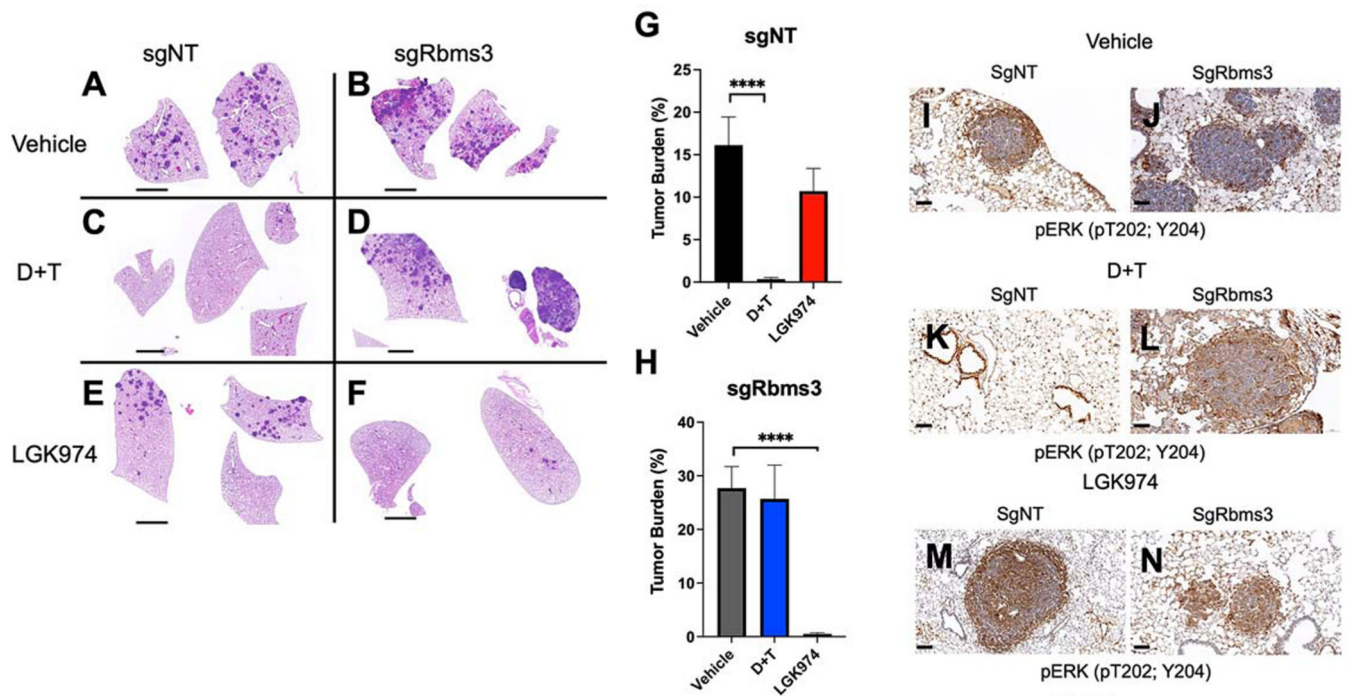


Figure 7: *Rbms3* silencing drives resistance to pathway-targeted inhibition of BRAF^{V600E} while adapting sensitivity to inhibition of Porcupine.

A: Representative images of H&E stained lung sections harvested 11 weeks post initiation from *BC* mice following treatment with the indicated pharmacological agents starting at 6 weeks post initiation with 5×10^4 pfu lenti-CRE. *BC* mice were dosed once daily for 5 weeks with: 1. Vehicle control; 2. dabrafenib (75 mg/kg) plus trametinib (1 mg/kg) or; 3. LGK974 (5mg/kg). **B&C:** Quantification of lung tumor burden in *BC* mice initiated with sgNT-CRE or sgRbms3-CRE and dosed with the indicated pharmacological agents as indicated. Mean tumor burden is graphed, and error bars represent SEM. N= 5–7 mice per dosing arm. Statistical analysis was performed using a one-way ANOVA (**** = $p < 0.0001$.)

Table 1.

Trunk CIS genes involved in lung adenocarcinoma progression of BRAF^{V600E}-initiated tumors. CIS genes containing 5 or more sequence read counts per tumor from 3 or more tumors and have corrected $p < 0.05$ by gCIS analysis.

Gene	p value (adj)
<i>Cux1</i>	3.25E-99
<i>Wapal</i>	1.24E-79
<i>Top1</i>	1.50E-71
<i>Cmip</i>	5.90E-50
<i>Gnaq</i>	5.74E-23
<i>Snd1</i>	3.75E-14
<i>Foxp1</i>	1.73E-11
<i>Rbms3</i>	4.99E-03

Author Manuscript

Author Manuscript

Author Manuscript

Author Manuscript